Wind field risk aware Global Path Planning and Trajectory Optimization in Urban Low-altitude Environments

Sichang Wang [1], Leyang Zhao [1], Xiaoming Li [1], Hang Mei [1], Lei Han [1], Yang Zhao [1], Ding Ma [1]

[1] Research Institute for Smart Cities, School of Architecture and Urban Planning, Shenzhen University, Shenzhen, 518060, PR China – wsichang@outlook.com

Keywords: Urban low-altitude environment; Unmanned aerial vehicle; Wind field simulation; Wind risk-aware path planning; Digital Twins for Mobility

Abstract:

Urban building clusters can significantly alter the low-altitude urban wind field, creating local regions with high wind speed, intense turbulence, and strong non-uniform disturbances. These conditions may cause lateral deviation, attitude instability, increased trajectory error, and even exceed the wind-resistance limits of low-altitude UAVs. To address the lack of explicit modeling of local high-risk wind regions in traditional path planning methods, this paper proposes a wind-risk-aware path planning method, termed RP- A* (Wind Risk-Aware Probability A*). First, a steady-state RANS urban airflow model with the standard k-ε turbulence model is used to obtain the mean wind field and turbulence statistics in the low-altitude flight region. Second, the CFD results are reconstructed on a grid to build a wind risk model consisting of gust risk, crosswind risk, and overall wind-limit-exceedance risk. Third, a direction-dependent integrated risk cost is introduced into the A* search framework, and the RP-A* algorithm is developed to achieve path planning that balances route efficiency and flight safety. Finally, Monte Carlo simulations driven by turbulence-based wind perturbation samples are conducted to estimate the empirical failure rate of planned paths. Results show that RP-A* significantly reduces path failure risk compared with baseline shortest-path methods while requiring only a limited increase in path length. The proposed framework provides an effective approach for safe UAV path planning in complex urban low-altitude environments.

1. Introduction

In recent years, the development and utilization of low-altitude airspace resources have gradually moved from conceptual exploration to practical deployment. The demand for UAV applications in urban logistics, security inspection, power line patrol, traffic monitoring, and disaster emergency response continues to grow (Blocken and Carmeliet, 2004). However, as mission areas extend from open suburban regions to densely built urban areas, the environmental uncertainty encountered during flight increases significantly. Among these factors, the complex wind field induced by urban building clusters is one of the most critical. Through blockage, deflection, acceleration, separation, and reattachment of the incoming airflow, complex buildings generate strongly non-uniform wind structures in low-altitude regions (Toparlar et al., 2017). As a result, UAVs may still encounter unpredictable wind disturbances even along paths that appear geometrically feasible. This has become one of the key factors limiting the safety and reliability of autonomous low-altitude flight in urban environments (Yang et al., 2023).

From the perspective of flight dynamics, UAVs, especially multirotor platforms, are highly sensitive to the near-ground wind environment. Strong headwinds or tailwinds may increase propulsion load and energy consumption. Sudden gusts can cause attitude disturbances and large control fluctuations (Sezer et al., 2023). Crosswinds directly affect trajectory tracking, lateral control, and attitude stability. At the block scale, these problems are not determined solely by the mean wind speed. They are also closely related to local turbulence enhancement, wake recirculation, and crosswind exposure under different path directions caused by building clusters. In other words, even when two candidate paths have similar geometric lengths, their levels of wind exposure may differ significantly. Therefore, path planning for urban low-altitude flight should not be regarded simply as obstacle avoidance or shortest-path search. Instead, it should be treated as a multi-factor decision problem under both environmental and flight-safety constraints (Techy and Woolsey, 2009).

However, from the perspective of urban wind-related safety constraints, most classical planning algorithms are still mainly based on geometric distance or travers ability (Chakrabarty and Langelaan, 2013). Even in studies that incorporate wind information, the mean wind speed magnitude is often used only as an additional cost term. In essence, such methods remain at the heuristic level of assuming that regions with stronger winds are less favourable for traversal. This may be reasonable in open areas or weak-disturbance scenarios, but it has clear limitations in complex low-altitude wind fields induced by urban buildings (Gu et al., 2025). First, the mean wind speed cannot adequately capture the sudden risks caused by local fluctuating winds. Second, crosswind exposure is strongly direction-dependent, and the hazard level at the same location may vary with flight heading. Third, because the cost function lacks an effective mapping from high-resolution flow-field features and multidimensional ground-risk costs to planning penalties, the shortest path generated by the planner may pass directly through the core regions with intense wind disturbance or dense population below (Wang et al., 2025).

Therefore, UAV path planning in urban environments needs to move beyond geometric feasibility toward wind-safe feasibility. This shift means that a path planning algorithm should not only determine whether a region can be traversed, but also evaluate the probability of encountering unacceptable wind disturbances when passing through that region and whether such risk depends on the current flight direction. First, computational fluid dynamics should be used to obtain urban near-ground wind fields with sufficient spatial resolution. Second, risk-related quantities relevant to UAV flight safety should be extracted from

CFD outputs such as mean wind speed and turbulent kinetic energy. Third, these risk quantities should be reconstructed into a regular map representation and embedded into a heuristic path-search framework. Finally, an independent statistical validation mechanism, separate from the planning cost function itself, is needed to verify whether the planned path indeed exhibits a lower actual failure probability under random wind disturbances. To address these issues, this paper proposes a wind-risk-aware path planning method, termed RP-A* (Wind-Risk-Aware Probability A*). The main contributions are as follows.

(1) We propose a risk modeling scheme that converts physical wind-field variables into probabilistic indicators more directly related to flight safety, thereby improving the interpretability of environmental representation.

(2) We distinguish direction-independent and direction-dependent risks, and discretize crosswind risk over candidate expansion directions, allowing the planner to select safer paths according to flight heading.

(3) We incorporate risk avoidance into both path planning and Monte Carlo validation, where a flight is considered failed if any path point exceeds the prescribed limit, enabling evaluation of the actual safety of the entire path.

Overall, this work aims to develop a safe path planning method for low-altitude UAV operations in urban environments that balances physical soundness, algorithmic practicality, and validation comparability.

2. Related Work

2.1 Urban Microclimate Wind Field Simulation

Research on urban microclimate and wind environments around buildings has developed a mature computational fluid dynamics (CFD) framework. Early studies focused on flow mechanisms around buildings, wind-tunnel comparisons, and numerical simulation guidelines for engineering applications. Typical issues in pedestrian-level wind environments and practical CFD applications have been systematically reviewed, including mesh generation, boundary conditions, turbulence modelling, and validation procedures (Blocken and Carmeliet, 2004; Tominaga et al., 2008). Subsequent reviews further clarified the applicability, advantages, limitations, and engineering feasibility of steady RANS, URANS, and LES for building wind environments and urban microclimate prediction (Blocken et al., 2016; Toparlar et al., 2017). These studies established the theoretical and methodological foundation for simulating wind fields in urban building clusters and showed that CFD can capture key phenomena such as building-induced flow separation, street-canyon acceleration, wake formation, and local turbulence enhancement.

As the research scale expanded from isolated buildings to real neighbourhoods and urban districts, greater attention was given to geometric realism, surrounding-building effects, multiscale coupling, and model validation. Full-scale community models and surrounding-building sensitivity analyses have shown that simplified geometry or insufficient upstream context may lead to biased local wind-speed estimates (Liu et al., 2017; Zheng et al., 2021). CFD validation studies under different climatic conditions also indicate that model parameters and physical process treatments require careful adjustment for different urban environments (Brozovsky et al., 2021; Kim and Lee, 2024). Recent reviews further suggest that urban microclimate simulation is evolving from pure wind prediction toward coupled analysis involving thermal environments, building energy, multiphysics processes, and data-driven surrogate models (Yang et al., 2023; Sezer et al., 2023). Meanwhile, UAV-related studies have begun to combine multiscale urban modelling, UAV observations, automated CFD workflows, weather forecasts, and geospatial data to support low-altitude wind-field reconstruction (Hang et al., 2024; Suárez-Vázquez et al., 2025). These studies suggest that it is now technically feasible to obtain mean wind speed and turbulence statistics with relatively high spatial resolution for complex urban low-altitude environments.

2.2 Wind-Aware Path Planning Methods

Research on UAV path planning in windy environments has evolved from idealized wind fields to more complex environmental conditions. Early studies mainly treated wind as an external factor affecting flight time, turning constraints, energy consumption, or path tracking. These works extended UAV planning to time-varying wind fields, structural inspection missions, urban path following, surveillance tasks, and joint task allocation–path optimization under wind disturbances (Chakrabarty and Langelaan, 2013; Guerrero and Bestaoui, 2013; Kothari et al., 2014; Zhang et al., 2014; Luo et al., 2018). They laid the foundation for wind-constrained path planning, but most still relied on simplified wind descriptions, such as uniform wind, steady wind, or low-dimensional wind models. Their main focus was time optimality, route efficiency, or trackability, rather than fine-grained flight-safety risks caused by complex building-induced urban wind fields.

In recent years, wind-constrained path planning has gradually moved toward realistic scenarios, low-altitude urban environments, and safety-oriented evaluation. Existing studies have investigated wind-resistant path planning for offshore ship reconstruction, UAS path evaluation in building-cluster wind fields, energy-optimal 3D flight planning in realistic urban wind fields, and UAV decision-making under environmental uncertainty (Liu et al., 2022; Nathanael et al., 2023; Rienecker et al., 2023; Hu et al., 2024). Other studies have explicitly incorporated urban wind resistance, turbulence, CFD-based route evaluation, and wind-induced threat identification into UAV planning or safety assessment (Gu et al., 2025; Wang et al., 2025; Liu et al., 2026). These works indicate that the field is moving from simply considering wind as a cost factor toward explicitly identifying and avoiding wind-field risks.

Overall, existing studies have achieved substantial progress in both high-resolution urban wind field simulation and wind-constrained path planning. However, there is still a clear gap between these two research lines. First, urban microclimate studies can provide rich outputs such as mean wind speed, flow direction, and turbulent kinetic energy, but these results are mainly used for pedestrian wind comfort, ventilation potential, thermal environment analysis, or building design optimization, and have not yet been systematically transformed into computable risk quantities for UAV flight safety. Second, although existing wind-constrained path planning studies have started to use CFD or statistical wind data, many methods still rely mainly on mean wind speed, energy correction, or no-fly-zone construction, with insufficient distinction among gust disturbance, direction-dependent crosswind, and platform wind-limit exceedance. Third, although many studies have used wind-related costs in path planning, relatively few have combined local risk modeling with statistical failure validation of the entire path. Based on this gap, the present study starts from urban CFD wind fields, further represents the wind environment in terms of gust risk, crosswind risk, and overall wind-limit-exceedance risk, and embeds these factors into both path search and Monte Carlo posterior validation. In this way, the study connects wind field simulation, risk modeling, safe path planning, and statistical validation into a more complete technical framework.

3. Methods

This study first obtains the physical basis data of the UAV flight environment through numerical simulation of the urban wind field. It then converts CFD outputs, such as mean wind speed and turbulent kinetic energy, into measurable, comparable, and callable flight risk indicators. Finally, the direction-dependent integrated risk is introduced into the process of global path planning and trajectory optimization, so that the planned path no longer pursues only geometric shortest distance, but instead balances path efficiency and flight safety under obstacle and travers ability constraints.

3.1 Urban Microclimate Wind Field Simulation

The main purpose of the numerical simulation is not to reproduce complex local vortex structures around building surfaces, but to obtain the mean wind field distribution and turbulence statistics that are relevant to low-altitude flight safety. To this end, OpenFOAM is adopted as the wind field solver. The three-dimensional building surface model of the study area is imported into the computational domain, and a sufficiently large external flow bounding box is constructed to ensure that inflow development, disturbance propagation through the building cluster, and downstream recovery can all evolve within a reasonable spatial range. This setup helps reduce the influence of boundary conditions on the wind distribution in flight region.

In terms of geometric modelling, the urban buildings in the study area are imported into the computational domain in the form of three-dimensional surface models, and the domain is constructed using an external flow bounding box. The building cluster is placed in a sufficiently large three-dimensional domain to provide reasonable separation among the inflow region, the building-induced disturbance region, and the outflow recovery region, thereby reducing nonphysical interference from boundary conditions in the core study area. Since the subsequent analysis focuses on the external low-altitude flight region rather than wall-attached flight or local impact on building surfaces, the key point of geometric processing is to preserve the overall spatial morphology of the building cluster, the dominant height variations, and the street-canyon structure, rather than pursuing extremely fine reconstruction of building corners and surface details. This treatment makes it possible to resolve the dominant flow structures while controlling computational cost, thus ensuring engineering practicality and supporting simulations under multiple conditions.

For turbulence modelling, the steady Reynolds-averaged Navier–Stokes (RANS) method is adopted together with the standard k-ε turbulence model to describe the mean turbulent effects in building airflow. This choice is based on three considerations. First, the standard k-ε model directly provides turbulent kinetic energy k and dissipation rate ε, which are required for subsequent risk modelling and facilitate the transition from mean flow results to a probabilistic risk model. Second, for the analysis of mean wind environments in large-scale urban external flows, this model has mature engineering applicability and offers a reasonable balance between computational accuracy and efficiency. Third, compared with high-cost transient methods such as LES, steady RANS is more suitable for batch simulations under multiple wind directions and inflow conditions, which is beneficial for later path-planning experiments and parameter sensitivity analysis. For boundary conditions, the inlet is prescribed with inflow velocity and corresponding turbulence parameters, the outlet is set as a pressure reference boundary, and the building surfaces and ground are treated as wall boundaries. By adjusting the inflow wind speed and horizontal wind direction, different wind conditions can be generated to analyze how urban building clusters affect the low-altitude wind field under different prevailing wind conditions.

After the simulation is completed, several key physical variables are extracted from the CFD results, including the mean wind velocity vector $U = (U_x, U_y, U_z)$, the mean wind speed magnitude$|U|$, turbulent kinetic energy k, and dissipation rate ε. The mean wind velocity vector is used to characterize the background wind distribution and flow deflection in the building-cluster environment. The mean wind speed magnitude reflects the locations of local high-speed and accelerated flow regions. Turbulent kinetic energy is used to measure the intensity of local wind disturbances and serves as a core parameter for constructing the random fluctuating wind model. The dissipation rate is used to further describe turbulence scale information.

3.2 Random Wind Risk Modelling and Construction of an Integrated Risk Metric

After obtaining the regularized urban wind field, this study further addresses the problem of how to convert CFD-derived physical variables into UAV safety risks. A random wind risk modelling framework is proposed, in which wind risk in urban low-altitude environments is divided into three categories: gust risk, crosswind risk, and overall wind-limit-exceedance risk. Based on these three components, a unified integrated risk metric is constructed. In this way, wind-field variables with fluid-dynamics meaning are further transformed into probabilistic quantities with direct flight-safety meaning, enabling an effective transition from environmental information to planning cost. The overall random wind risk modelling framework is shown in Figure 1.

To construct probabilistic risks from the mean wind field and turbulence statistics, the local instantaneous wind is expressed as

https://doi.org/10.5194/isprs-archives-XLIX-B4-2026-453-2026

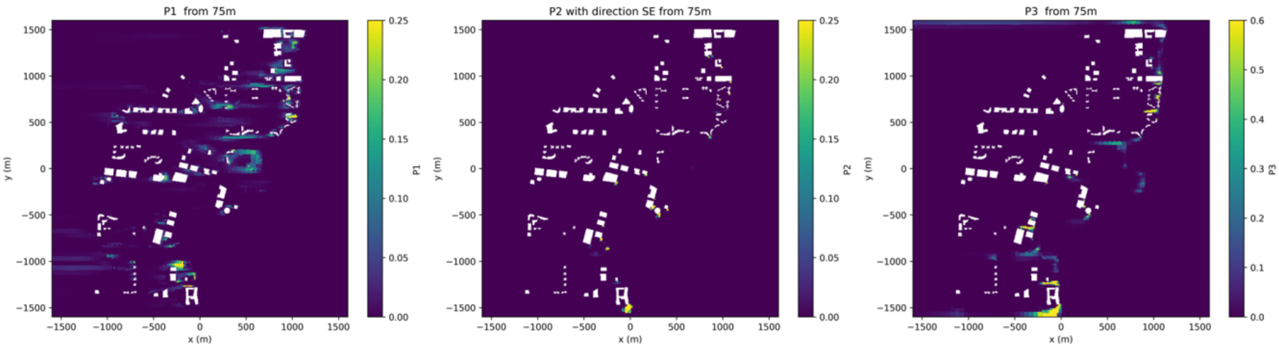

Figure 1: Random Wind Risk Modelling in typical high-density urban area.

the sum of the mean wind and a random disturbance term, namely:

$$W = U + \epsilon \tag{1}$$

where U is the local mean wind velocity vector provided by CFD, and ϵ is a random disturbance term representing local fluctuating wind. Since the focus of this study is an engineering-oriented risk model for path planning rather than exact reconstruction of the full high-frequency transient turbulence process, an isotropic Gaussian disturbance assumption is adopted. Specifically, the random disturbances in the three coordinate directions are assumed to have identical statistical properties. Under this assumption, the variance of each fluctuating wind component is determined by the local turbulent kinetic energy, and the corresponding single-axis standard deviation can therefore be directly obtained from k.

Among the three risk types, the first is gust risk, which is used to characterize the probability that the magnitude of T_g. The gust risk is defined as:

$$P_1 = P\big(|\epsilon| > T_g\big) \tag{2}$$

This probability indicates whether the turbulent fluctuation itself is large enough to cause significant impact on UAV attitude control, trajectory keeping, and flight stability. Since ϵ is modeled as an isotropic Gaussian random vector, its magnitude follows a Maxwell-type distribution, and P_1 can therefore be computed once σ_u is known. Physically, gust risk emphasizes the intensity of local disturbance rather than the mean wind speed itself, and is closely related to turbulent kinetic energy. In regions where the mean wind speed is not necessarily the highest but local turbulence is very strong; gust risk can provide a more sensitive safety indicator than mean wind speed alone.

The second type is crosswind risk, which describes the probability that the lateral wind component exceeds a threshold for a given flight direction. Let d denote the unit heading vector of a path segment, and let n be the corresponding lateral unit vector. The projection of the local instantaneous wind onto the lateral direction is then given by:

$$W_\perp = n^T W \tag{3}$$

Let the crosswind threshold be T_c. The crosswind risk defined as

$$P_2 = P(|W_\perp| > T_c) \tag{4}$$

Crosswind risk depends not only on the local wind field itself, but also on the current flight direction of the path. This means that, at the same spatial location, the crosswind hazard level may differ under different flight headings. In this study, P_2 is calculated for a predefined set of discrete directions to form a direction-dependent risk table. This design allows the planner to directly query the corresponding crosswind risk for a given expansion direction during search, without repeatedly performing online probabilistic derivation, thus balancing physical rationality and computational efficiency.

The third type is overall wind-limit-exceedance risk, which measures whether the local instantaneous total wind speed may exceed the platform's wind-resistance limit. Let $V_{\max}$ denote the maximum total wind speed that the UAV platform can withstand. The overall wind-limit-exceedance risk is defined as:

$$P_3 = P(|W| > V_{\max}) \tag{5}$$

Unlike gust risk, which mainly reflects the magnitude of fluctuating wind, P_3 is affected by both the mean wind and the random disturbance. It indicates whether the overall wind-safety margin of the platform is exceeded. If the mean wind speed in a region is already high, the overall wind-limit-exceedance risk may still become large even when turbulence is not particularly strong. Therefore, P_3 directly characterizes the combined wind load acting on the platform relative to its overall flight capability.

To integrate these three risks within a unified framework, an integrated risk metric is further constructed. The total wind threshold $V_{\max}$ directly corresponds to the upper limit of the platform's wind-resistance capability, while the crosswind threshold T_c and the gust threshold T_g are treated as control-margin boundaries derived from the total wind threshold and are generally lower than $V_{\max}$. The integrated risk is then defined as:

$$R = \alpha(w_1P_1 + w_2P_2 + w_3P_3) + (1-\alpha)\max(P_1, P_2, P_3) \tag{6}$$

Where w_1, w_2, w_3 are the combination weights of the three risk types, and α is the balance coefficient between the weighted-average term and the extreme-value enhancement term.

Based on this formulation, two types of risk layers are finally obtained. The first type is the direction-independent risk layer, which includes gust risk P_1 and overall wind-limit-exceedance risk P_3. The second type is the direction-dependent risk layer, which includes the crosswind risk P_2^{dir} and the integrated risk R^{dir} under each discrete direction. At the same time, each grid cell is organized into a unified data structure that contains three categories of information: basic wind-field information, risk information, and constraint information. The basic wind-field information includes $U_x, U_y, U_z, U_{mag}, k, \varepsilon, \sigma_u$. The risk information includes $P_1, P_3, P_2^{dir}, R^{dir}$. The constraint information includes the obstacle mask and the hard no-fly mask.

3.3 Wind-Risk-Aware Global Path Planning and Trajectory Optimization

After completing the urban wind field simulation and random wind risk modeling, this study further proposes a wind-risk-aware method for global path planning and trajectory optimization. The core idea is that, under obstacle constraints and wind-based travers ability constraints, the planner no longer seeks only the geometrically shortest path. Instead, it explicitly incorporates direction-dependent integrated risk into the global search process, so that the planned path can actively avoid regions with high wind speed, strong turbulence, and high crosswind exposure, thereby achieving a better balance between safety and efficiency.

In this study, not all non-building areas are regarded as flyable space. Instead, hard wind-environment constraints are further imposed to define a more realistic traversable domain. Specifically, a candidate grid cell is allowed to enter the search only if it satisfies all of the following conditions: first, it does not belong to the building body or its safety buffer zone; second, it does not lie in a high-turbulence no-fly region where turbulent kinetic energy exceeds the prescribed threshold; third, it does not lie in a high-wind-speed no-fly region where the mean wind speed exceeds the safety threshold. In this way, a two-level feasibility screening mechanism is established, consisting of geometric obstacle constraints and hard wind-field constraints. Compared with traditional methods that search for the shortest path only on a geometric map, this mechanism removes obviously unsafe regions before the search starts, thereby reducing the possibility that the planned path passes through strongly disturbed areas.

For the global search strategy, the A* algorithm is adopted as the basic framework, and direction-dependent integrated risk is embedded into the step cost. Let ds denote the geometric step length from the current node to a neighboring node. If the integrated risk of the target grid cell under the current expansion direction is R, then the single-step cost is defined as:

$$cost = ds \cdot (1 + \lambda R) \tag{7}$$

where λ is the risk weight parameter that controls the relative preference between efficiency-oriented planning and safety-oriented planning. When $\lambda = 0$, the algorithm reduces to the traditional shortest-path search based purely on geometry. As λ increases, the step cost in high-risk regions is further amplified, and the search becomes more likely to avoid dangerous areas and select alternative routes that are slightly longer but safer. Therefore, λ serves as the key parameter that maps risk representation into path selection behavior and enables the trade-off between safety and efficiency.

To maintain the stability and interpretability of heuristic search, no additional future risk prediction is introduced into the heuristic function. Instead, the Euclidean distance from the current node to the goal node is still used as the heuristic, namely:

$$h(n) = \|X_{\mathrm{n}} - X_{\mathrm{goal}}\|_2 \tag{8}$$

On the one hand, the Euclidean distance provides a natural lower-bound estimate of the remaining path length and helps preserve the efficiency of A*. On the other hand, if prior risk information of future regions were included in the heuristic, inaccurate far-field risk estimation might distort the heuristic and even affect search stability. Therefore, the influence of risk is concentrated in the accumulated cost $g(n)$. During node expansion, the planner obtains local risk penalties through direct lookup from the risk table, rather than relying on rough prediction of future regions. This treatment reduces the complexity of heuristic design and improves the engineering robustness of the method.

The algorithm proceeds as follows. First, the wind-field grid map and the risk grid map are loaded, and the obstacle mask, hard-constraint mask, and direction-dependent integrated risk table are obtained. Next, the OPEN list, CLOSED list, start-node cost, and parent-node mapping are initialized. During the search, the node with the smallest $f = g + h$ value is extracted from the OPEN list as the current node. If it reaches the goal, the parent-node sequence is traced back to output the path. Otherwise, each neighboring node of the current node is examined in turn for boundary violation, obstacle occupancy, and wind-based no-fly conditions. If the travers ability constraints are satisfied, the integrated risk value R^{dir} of the target neighboring node under the current expansion direction is obtained by directional lookup. The single-step risk-weighted cost is then computed, and the accumulated cost g is updated. When the new path is better than the recorded one, the parent node and the values of g h, and f are updated, and the neighboring node is inserted into the OPEN list. If the OPEN list is exhausted before the goal is reached, it means that no feasible connected path exists between the start and the goal under the current constraints. In this way, the conventional objective of minimizing distance in the A* framework is extended to minimizing the combined cost of distance and risk, thereby enabling global path planning for safety in urban wind environments.

At the trajectory optimization level, the method also outputs several evaluation metrics, including total path cost, geometric length, number of expanded nodes, peak OPEN-list size, and planning time, providing a basis for comparing trajectory quality under different algorithms and parameter settings. In addition, the mean wind speed profile, integrated risk profile, and locations of local risk peaks can be extracted along the path to identify potentially unsafe segments. This treatment means that the planning result is no longer just an abstract list of nodes, but a flight trajectory representation that can be analyzed, evaluated, and further optimized. Although this study mainly focuses on global path search itself, by mapping the path sequence into the physical coordinate space and combining it with risk-profile analysis, interfaces are already reserved for future trajectory smoothing, control-constraint matching, and local maneuver

https://doi.org/10.5194/isprs-archives-XLIX-B4-2026-453-2026

optimization.

4. Experiments

To verify the effectiveness of the proposed wind-risk-aware path planning method in complex urban low-altitude environments, experiments were conducted from three aspects: risk-field modelling, sensitivity to the risk weight parameter, and comparison with different planning algorithms. First, a typical high-density urban area of about 6 km² in Yuehai Subdistrict, Nanshan District, Shenzhen was selected for wind-field modelling, and the spatial characteristics of the urban wind environment at different flight altitudes were analysed. Second, under the same start and goal points and environmental constraints, the effects of the risk weight parameter λ on path shape, planning success rate, path length, planning time, and the number of expanded nodes were investigated to identify a reasonable balance between safety and efficiency. Finally, the proposed RP-A* algorithm was compared with A*, Bi-A*, Theta*, JPS, and a simple wind-aware path planning algorithm in terms of path length and failure rate, so as to evaluate its performance under urban wind-field constraints.

To assess the actual safety of planned paths under stochastic wind disturbances, a Monte Carlo-based posterior validation procedure was further designed. For each path, local mean wind and turbulent kinetic energy were extracted from the CFD-derived wind field, and random wind perturbations were generated according to the local turbulence statistics to construct stochastic wind realizations. In each trial, the wind condition was checked point by point along the path, and the trial was marked as a failure if any operational limit was exceeded at any path point. After repeated simulations, the empirical failure rate was calculated as the ratio of failed trials to the total number of Monte Carlo trials. The same validation procedure was applied to all compared algorithms to ensure a fair safety assessment.

4.1 Visualization Results of Risk-Field Modelling

Figure 2 shows the study area selected for wind-field modelling and path-planning experiments. A region of about 6 km² in Yuehai Subdistrict, Shenzhen was selected as the experimental scenario. This area has a high building density and large height variations. It contains local super-high-rise clusters, and can therefore represent the complexity of a typical urban core area for low-altitude UAV flight. Considering that UAV missions in urban environments often operate at different altitude levels, wind-field modeling was carried out at 50 m, 75 m, and 100 m, and the corresponding risk fields were further constructed based on the CFD results. Figure 3 shows the visualization results of the wind field and risk field at these three heights.

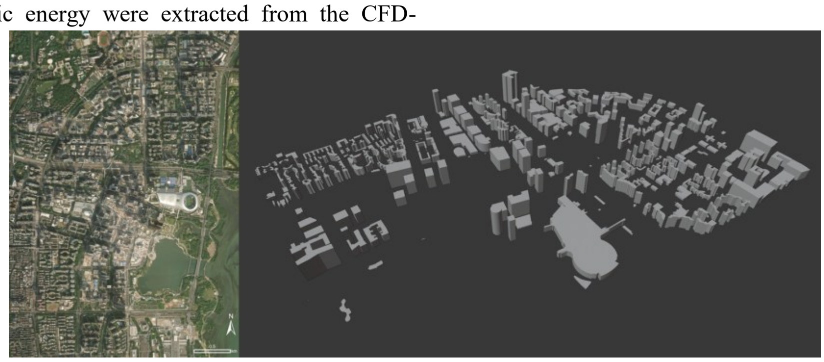

Figure 2: Schematic diagram of the study area.

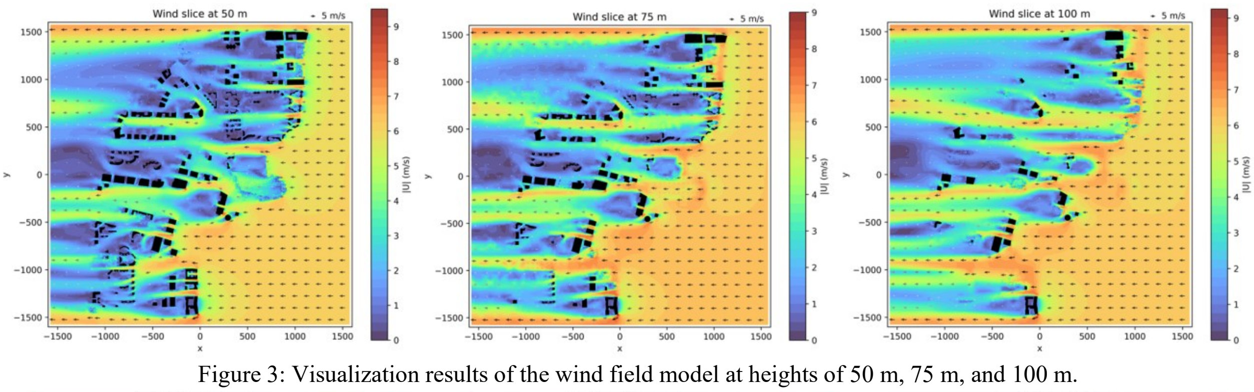

Figure 3: Visualization results of the wind field model at heights of 50 m, 75 m, and 100 m.

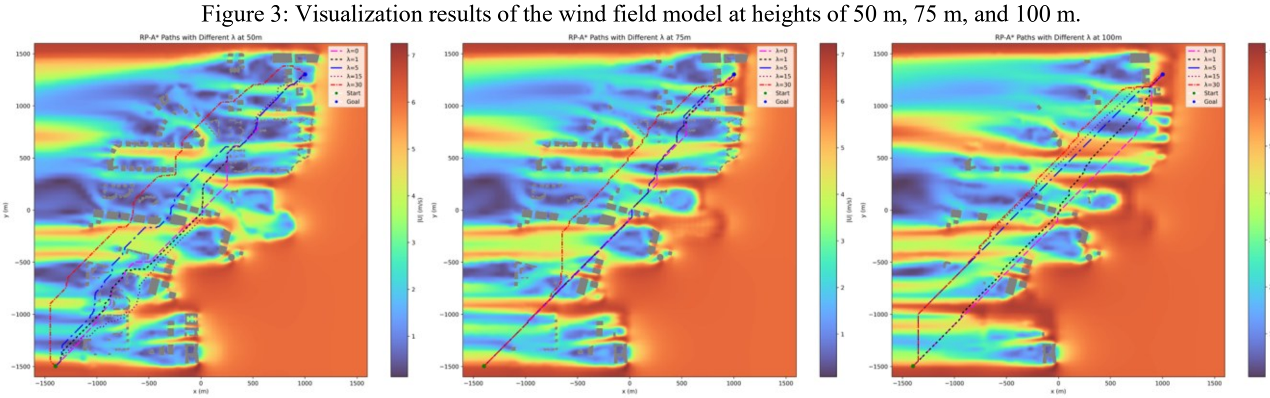

Figure 4: Comparison of path planning results under different values of the risk weight parameter λ.

As shown in Figure 3, the proposed method can clearly capture the wind-environment characteristics of the study area at different altitudes. In general, the disturbance of incoming flow by building clusters is evident at all three height levels, although the influence patterns differ. At 50 m, the wind field is most strongly affected by building blockage, flow deflection, and street-canyon channeling. Local wind-acceleration zones, leeward recirculation regions, and high-turbulence areas are distributed in a scattered manner, showing strong spatial non-uniformity. At 75 m, the direct influence of some mid- and low-rise buildings becomes weaker, but strong local wind-speed gradients and wake disturbances still appear around high-rise clusters. At 100 m, the overall wind field becomes relatively smoother, but significant acceleration and downwash effects still exist around super-high-rise buildings. This indicates that even at higher flight layers, complex urban morphology still has a non-negligible impact on UAV flight safety.

From the spatial distribution, high-risk regions are mainly concentrated near the windward sides of high-rise buildings, in narrow passages between densely built structures, and in large-scale leeward wake regions behind building clusters. These areas usually exhibit strong wind-speed gradients, obvious wind-direction deflection, and high turbulence intensity, all of which are unfavorable for UAV trajectory tracking and attitude control. In contrast, some areas with larger building spacing and relatively open surroundings show much lower risk values and may form potential low-risk transit corridors. These results indicate that the proposed method can not only reconstruct the urban low-altitude wind environment of the study area with reasonable realism, but also further transform raw CFD results into risk-distribution maps with explicit flight-safety meaning, thereby providing effective environmental input for subsequent path planning.

4.2 Effect of Different λ Values on Path Planning Results

In the proposed method, the risk weight parameter λ determines the strength of wind risk in the path cost. A larger λ makes the planner more likely to avoid high-risk regions, whereas a smaller λ makes the path closer to the geometric shortest path of conventional A*. Therefore, λ directly reflects the trade-off between path efficiency and flight safety.

Figure 4 shows the path planning results under different values of λ. As λ increases, the path responds more strongly to the risk field. When $\lambda=0$, the algorithm is equivalent to standard A*, and the path mainly follows the geometric shortest direction. Although the path is relatively direct, it passes through some regions with high wind speed and strong disturbance, indicating that the geometric shortest path is not necessarily the safest one. When λ increases to 1 and 5, the path begins to actively avoid local high-risk areas while still maintaining good accessibility and without obvious detours. This shows that the risk term has already become effective in the decision process. When λ=20 and 50, the path becomes much more conservative. In particular, when $\lambda=50$, the planned path almost completely avoids all regions with wind speed greater than 5 m/s, indicating that the risk constraint has become the dominant factor.

Figure 5 illustrates the effects of different λ values on path failure rate, path length, planning time, and the number of expanded nodes. In terms of safety, when λ=0, the path failure rate is about 50%, indicating that planning solely according to the geometric shortest path is not suitable for complex urban wind environments. As λ increases, the failure rate decreases rapidly. When $\lambda\geq5$, the failure rate drops below 10%, showing that the introduction of wind-risk cost can significantly improve the statistical safety of the planned path. In terms of path length, the overall path length increases with λ, especially when $\lambda\geq10$, with an average increase of about 20 m. This suggests that in complex wind environments, safer paths usually require some detour cost.

In terms of computational cost, both planning time and the number of expanded nodes increase with λ. When λ=0, the planning time is the shortest, about 0.8 s. When $\lambda>10$, the planning time exceeds 1 s, and the number of expanded nodes also increases significantly. This is because once high-risk regions are assigned larger penalties, the originally direct route is no longer optimal, and the search has to explore more candidate branches, which increases the computational burden. In other words, an excessively large λ can further reduce risk, but it may also make the path overly conservative and reduce the real-time performance of the algorithm.

Overall, different values of λ correspond to different planning preferences. A smaller λ emphasizes efficiency but provides insufficient safety, whereas a larger λ emphasizes safety but causes longer paths and higher search cost. By comparison, λ=5 shows a good balance among failure rate, path length, planning time, and the number of expanded nodes. Therefore, λ=5 is adopted as the baseline parameter in the subsequent algorithm comparison experiments.

4.3 Performance of Different Path Planning Algorithms in the Study Area

After determining the parameter setting, the proposed RP-A* was further compared with A*, Bi-A*, Wind-aware A*, Theta*, and JPS. Figure 6 shows the planned trajectories of different algorithms in the study area, and Figure 7 summarizes their path failure rates and path lengths. The results clearly reflect the differences among these algorithms in path efficiency and risk control.
As shown in Figure 6, although A*, Bi-A*, and JPS differ in implementation, they all essentially take geometric distance optimality as the main objective, and therefore generate paths with similar spatial distributions. A* directly searches for the shortest path, Bi-A* improves efficiency through bidirectional search, and JPS reduces redundant expansions through pruning. However, none of these methods explicitly constrains wind risk. As a result, although their paths are relatively short, they are prone to passing through local high-risk regions, leading to relatively high failure rates in complex urban wind environments.

Theta* represents another planning strategy. By using line-of-sight connections, it reduces polyline turns and can therefore generate shorter and smoother paths. As seen in the figure, the trajectories of Theta* are usually closer to straight lines, and the local path shape is more natural. However, this geometric advantage does not necessarily imply higher safety. Since Theta* mainly optimizes path geometry without considering high-risk regions in the urban wind field, its paths are often more likely to pass directly through open areas and local dangerous zones. The

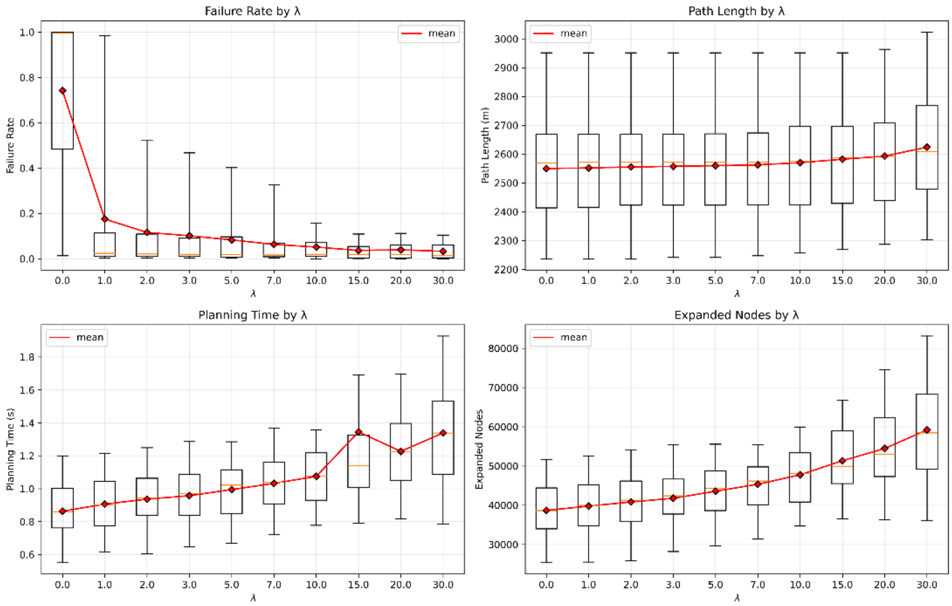

Figure 5: Influence of different values of the risk weight parameter λ on path planning performance metrics.

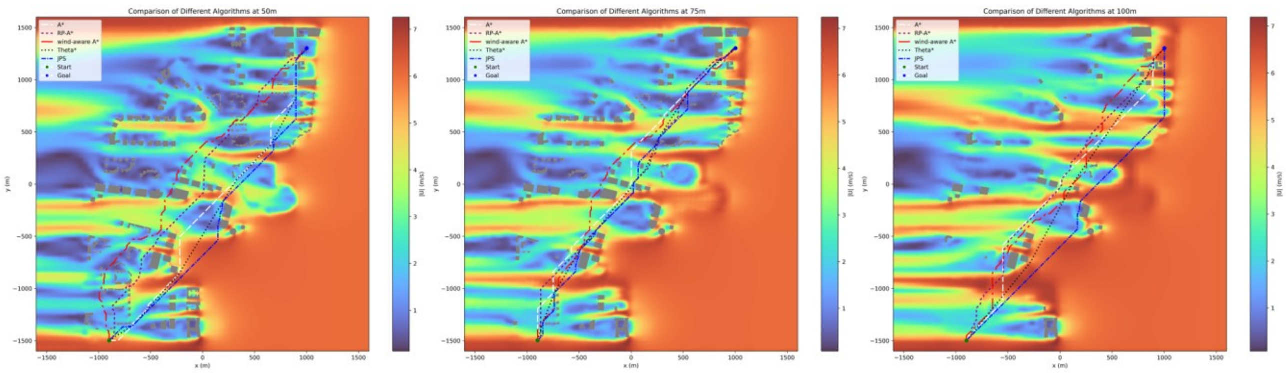

Figure 6: Comparison of trajectory results of different path planning algorithms in the study area.

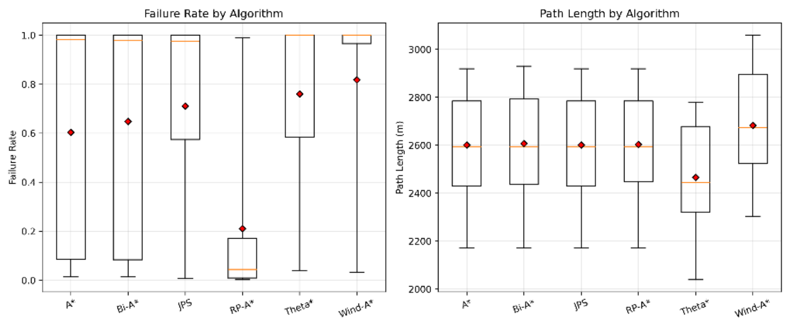

Figure 7: Comparison of path failure rate and path length for different path planning algorithms.

experimental results show that although Theta* has an advantage in path length, its safety is not improved accordingly. This suggests that geometric optimality is not equivalent to wind-environment safety.

Although Wind-aware A* introduces wind information into the path cost, its improvement remains limited. The main reason is that such methods usually penalize only the mean wind speed, which is essentially still a simplified strategy of assigning higher cost to stronger wind. In dense urban building areas, however, what truly affects UAV safety is not only the mean wind speed, but also local turbulent fluctuations, wake separation, and direction-dependent crosswind exposure. Since Wind-aware A* cannot explicitly represent these risks, it does not show clear advantages in either risk control or path length in this experiment.

In contrast, the proposed RP-A* demonstrates better overall performance. First, in terms of path failure rate, RP-A* clearly outperforms the other compared algorithms, indicating that the generated paths are more reliable in posterior random-wind validation. Second, in terms of path length, RP-A* is not the shortest, but it remains at roughly the same order of magnitude as A*, Bi-A*, and JPS, without excessive detours caused by pursuing safety. This indicates that the proposed method does not achieve safety simply by greatly increasing path length, but instead significantly reduces flight risk while maintaining relatively high path efficiency.

Mechanistically, the advantage of RP-A* mainly comes from its risk representation. The proposed method considers not only mean wind speed, but also gust risk, crosswind risk, and overall wind-limit-exceedance risk, enabling more comprehensive identification of local hazardous areas. In particular, crosswind risk is designed as a direction-dependent quantity, so that the same location may have different costs under different flight directions, allowing the planner to make more reasonable avoidance decisions. This feature is not available in A*, Bi-A*, JPS, Theta*, or simple Wind-aware A*. In addition, the integrated risk metric preserves both average-risk information and local extreme-risk information, enabling the search process to avoid globally high-risk regions while remaining sensitive to local danger peaks.

Overall, the trends shown in Figure 7 indicate that in complex urban low-altitude environments, traditional shortest-path methods, bidirectional acceleration methods, and any-angle path planning methods are all insufficient to fully satisfy flight-safety requirements. Wind-aware methods based only on mean wind-speed correction also have difficulty capturing the true risk accurately. By contrast, RP-A* can significantly reduce the failure rate while keeping the path length at an acceptable level, showing a better balance between safety and efficiency. This verifies the effectiveness of the proposed wind-risk-aware path planning method for safe UAV flight in urban low-altitude environments.

5. Conclusion

This study addresses the problem of safe UAV flight in complex urban low-altitude environments and proposes a wind-risk-aware path planning method following the main line of urban wind-field modeling, risk representation, and safe path planning. First, considering the strong disturbance of near-ground wind fields caused by dense urban building clusters, an urban microclimate wind-field model of the study area was established based on OpenFOAM, and key wind-field variables such as mean wind speed and turbulent kinetic energy were obtained at different flight altitudes. Second, based on these results, a random wind risk model was constructed, including gust risk, crosswind risk, and overall wind-limit-exceedance risk. An integrated risk metric was then developed to convert CFD-derived physical quantities into flight-safety risks. Finally, the integrated risk was incorporated into the A* search framework, and the RP-A* path planning method was proposed, enabling the planner to actively avoid high-risk regions while maintaining path efficiency.

The experimental results show that the constructed risk field can effectively reflect the spatial distribution characteristics of the wind environment in the complex building setting of the study area. Further algorithm comparison results compared with A*, Bi-A*, Theta*, JPS, and Wind-aware A*, the proposed method RP-A* significantly reduces the path failure rate while keeping the path length at an acceptable level, thus achieving a better balance between safety and efficiency.

Overall, this study demonstrates that in complex urban low-altitude environments, relying only on geometric shortest paths or simple mean-wind correction is insufficient to satisfy UAV flight-safety requirements. Explicitly incorporating multidimensional wind-risk information from urban wind fields into the path planning process can effectively improve path reliability. The proposed method provides a physically grounded and practically implementable solution for safe path planning of UAVs in urban low-altitude environments, and also lays a foundation for future research on three-dimensional trajectory optimization, dynamic wind-field updating, and validation on real flight platforms.

Reference

Blocken, B., Carmeliet, J., 2004. Pedestrian wind environment around buildings: Literature review and practical examples. Journal of Thermal Envelope and Building Science, 28(2), 107–159. https://doi.org/10.1177/1097196304044396.

Toparlar, Y., Blocken, B., Maiheu, B., et al., 2017. A review on the CFD analysis of urban microclimate. Renewable and Sustainable Energy Reviews, 80, 1613–1640. https://doi.org/10.1016/j.rser.2017.05.248.

Yang, S., Wang, L., Stathopoulos, T., et al., 2023. Urban microclimate and its impact on built environment—A review. Building and Environment, 238, 110334. https://doi.org/10.1016/j.buildenv.2023.110334.

Sezer, N., Yoonus, H., Zhan, D., et al., 2023. Urban microclimate and building energy models: A review of the latest progress in coupling strategies. Renewable and Sustainable Energy Reviews, 184, 113577. https://doi.org/10.1016/j.rser.2023.113577.

Techy, L., Woolsey, C.A., 2009. Minimum-time path planning for unmanned aerial vehicles in steady uniform winds. Journal of Guidance, Control, and Dynamics, 32(6), 1736–1746. https://doi.org/10.2514/1.44580.

Chakrabarty, A., Langelaan, J.W., 2013. UAV flight path planning in time varying complex wind-fields. Proceedings of the 2013 American Control Conference, Washington, DC, IEEE, 2568–2574. https://doi.org/10.1109/ACC.2013.6580221.

Gu, R., Zhao, Y., Ren, X., 2025. Integrating wind field analysis in UAV path planning: Enhancing safety and energy efficiency for urban logistics. Chinese Journal of Aeronautics, 39(1), 103605. https://doi.org/10.1016/j.cja.2025.103605.

Wang, J., He, X., Jiang, S., et al., 2025. Evaluation of urban wind effects on flight path planning of delivery drones using computational fluid dynamics simulations. Physics of Fluids, 37(8), 087124. https://doi.org/10.1063/5.0281373.

Tominaga, Y., Mochida, A., Yoshie, R., et al., 2008. AIJ guidelines for practical applications of CFD to pedestrian wind environment around buildings. Journal of Wind Engineering and Industrial Aerodynamics, 96(10–11), 1749–1761. https://doi.org/10.1016/j.jweia.2008.02.058.

Blocken, B., Stathopoulos, T., van Beeck, J.P.A.J., 2016. Pedestrian-level wind conditions around buildings: Review of wind-tunnel and CFD techniques and their accuracy for wind comfort assessment. Building and Environment, 100, 50–81. https://doi.org/10.1016/j.buildenv.2016.02.004.

Toparlar, Y., Blocken, B., Vos, P., et al., 2015. CFD simulation and validation of urban microclimate: A case study for Bergpolder Zuid, Rotterdam. Building and Environment, 83, 79–90. https://doi.org/10.1016/j.buildenv.2014.08.004.

Liu, S., Pan, W., Zhang, H., et al., 2017. CFD simulations of wind distribution in an urban community with a full-scale geometrical model. Building and Environment, 117, 11–23. https://doi.org/10.1016/j.buildenv.2017.02.021.

Zheng, S., Wang, Y., Zhai, Z.J., et al., 2021. Characteristics of wind flow around a target building with different surrounding building layers predicted by CFD simulation. Building and Environment, 201, 107962. https://doi.org/10.1016/j.buildenv.2021.107962.

Brozovsky, J., Simonsen, A., Gaitani, N., 2021. Validation of a CFD model for the evaluation of urban microclimate at high latitudes: A case study in Trondheim, Norway. Building and Environment, 205, 108175. https://doi.org/10.1016/j.buildenv.2021.108175.

Hang, J., Xu, Y., Hua, J., et al., 2024. A framework combining multi-scale model and unmanned aerial vehicle for investigating urban micrometeorology, thermal comfort, and energy balance. Sustainable Cities and Society, 115, 105847. https://doi.org/10.1016/j.scs.2024.105847.

Kim, G., Lee, G., 2024. Validation of CFD models of urban microclimates under high temperature and humidity conditions during daytime heatwaves in dense low-rise areas. Building and Environment, 266, 112087. https://doi.org/10.1016/j.buildenv.2024.112087.

Suárez-Vázquez, M., Varela Ballesta, S., Otero-Cacho, A., et al., 2025. A fast and automated approach for urban CFD simulations: Validation with meteorological predictions and its application to drone flights. Urban Climate, 64, 102664. https://doi.org/10.1016/j.uclim.2025.102664.

Guerrero, J.A., Bestaoui, Y., 2013. UAV path planning for structure inspection in windy environments. Journal of Intelligent & Robotic Systems, 69(1–4), 297–311. https://doi.org/10.1007/s10846-012-9778-2.

Kothari, M., Postlethwaite, I., Gu, D.W., 2014. UAV path following in windy urban environments. Journal of Intelligent & Robotic Systems, 74, 1013–1028. https://doi.org/10.1007/s10846-013-9873-z.

Zhang, X., Chen, J., Xin, B., 2014. Path planning for unmanned aerial vehicles in surveillance tasks under wind fields. Journal of Central South University, 21(8), 3079–3091. https://doi.org/10.1007/s11771-014-2279-7.

Luo, H., Liang, Z., Zhu, M., et al., 2018. Integrated optimization of unmanned aerial vehicle task allocation and path planning under steady wind. PLoS ONE, 13(3), e0194690. https://doi.org/10.1371/journal.pone.0194690.

Liu, T., Shen, R., Lei, Z., et al., 2022. Wind resistance aerial path planning for efficient reconstruction of offshore ship. International Journal of Digital Earth, 15(1), 1881–1904. https://doi.org/10.1080/17538947.2022.2140852.

Nathanael, J.C., Wang, C.H.J., Low, K.H., 2023. Simulation of wind field in a building complex for evaluation of the wind effect along UAS flight path. AIAA AVIATION 2023 Forum. https://doi.org/10.2514/6.2023-4096.

Rienecker, H., Hildebrand, V., Pfifer, H., 2023. Energy optimal 3D flight path planning for unmanned aerial vehicle in urban environments. CEAS Aeronautical Journal, 14, 621–636. https://doi.org/10.1007/s13272-023-00666-x.

Hu, Z., Chen, H., Lyons, E., et al., 2024. Towards sustainable UAV operations: Balancing economic optimization with environmental and social considerations in path planning. Transportation Research Part E: Logistics and Transportation Review, 181, 103314. https://doi.org/10.1016/j.tre.2023.103314.

Liu, Y., Shi, Y., Zhao, X., et al., 2026. Automatic helicopter flight based on wind-induced threat identification in urban environments. Chinese Journal of Aeronautics, 39(3), 103909. https://doi.org/10.1016/j.cja.2025.103909.